

Control of size and distribution of silicon quantum dots in silicon dielectrics for solar cell application: A review



Subhajit Dutta ^a, Somenath Chatterjee ^b, Kumar Mallem ^a, Young Hyun Cho ^{a,*}, Junsin Yi ^{a,**}

^a College of Information and Communication Engineering, Sungkyunkwan University, 2066 Seobu-ro, Jangan-gu, Suwon, Gyeonggi-do, 16419, South Korea

^b Center for Materials Science & Nanotechnology, Sikkim Manipal Institute of Technology, Sikkim Manipal University, Majitar, Sikkim, 737102, India

ARTICLE INFO

Article history:

Received 16 January 2018

Received in revised form

18 May 2018

Accepted 20 June 2018

Available online 26 June 2018

Keywords:

Silicon quantum dots

Size control

Growth parameter

Si QD solar cell

ABSTRACT

Nano-scale engineering for optoelectronic properties of silicon has shown its suitability in the modern era of Photovoltaic. The major focus is on Silicon quantum dots (Si QDs) which behave like an atom restricting the free movement of electrons. It provides an opportunity to control the energy states by manipulating the size of the Si QDs. Such closely packed Si QDs together form quasi-crystalline structures that lead to the formation of superlattices in different Si energy bands. Significant efforts have been devoted to the control of size and distribution density of the Si QDs. A current status of research efforts on the factors that influence the size and distribution density of Si QDs within the silicon-based matrix are discussed here. A brief summary of various fabrication techniques and mechanisms behind the growth of Si QDs are discussed in this study. A comparison on the effect of growth parameters for Si QDs with various dielectric/semiconductor matrix such as Silicon dioxide, Silicon nitride, Silicon carbide and the combination of the tandem solar cell is highlighted based on recent research progress. An overview towards the state of the art in the development, challenges and future trends of Si QDs to dictate as the third generation photovoltaic material are discussed in detail.

© 2018 Elsevier Ltd. All rights reserved.

1. Introduction

Recent developments in quantum dots (QD) technology have acquired lots of attention for the Photovoltaic (PV) application. Metaphoric to artificial atoms, QDs confine the three-dimensional movement of electrons within bound and discrete energy state. This confinement is due to the presence of interfacial interaction between semiconductor materials, the semiconductor surface, and electrostatic potentials due to doping, strain, impurities or combination of all these factors. Research is continuing to control those factors in order to engineer the electronic and photonic properties of QDs for third generation solar cell applications [1,2]. It was observed that the variation in size for QDs, the confinement regime changes which is supposed to be the key factor in circumventing the Shockley-Queisser limit of solar cell efficiency [3]. New studies have shown that maximum theoretical solar energy conversion by a single junction QD solar cell maybe efficient ~42% under AM 1.5

solar illumination for ~1.4 eV bandgap energy semiconductor [4]. Thus, in orders to achieve such high-performance device various QD materials, a promising candidate of great stature were studied and investigated [2].

At present, the photovoltaic market is mostly focused on the cost-effective enhancement of energy conversion of Si-based solar cells. Improving surface passivation, implementing new technology and exploring the nano regime of Si has been considered in this context [5–7]. In addition, the quantum confinement of Si showed interesting results that attracted researcher's attention. The indirect bandgap of Si showed promising performance equivalent to direct-bandgap materials providing easy access to bandgap tuning through different quantum structures [7–9]. Due to the decrease of the size of silicon nanocrystals (Si NCs), the optical spectrum was observed to have a blue shift with an enhancement in intensity which indicates not only the quantization of the bandgap but also the improvement for the radiative recombination rate in indirect transition mode [7,10,11].

Discovery of quantum confinement effect in porous silicon proved to be the gateway of progress in the development of Si NCs for advanced photovoltaic applications [7]. However, for PV applications Si QDs embedded in a Si-based dielectric/semiconductor

* Corresponding author.

** Corresponding author.

E-mail addresses: yhcho64@skku.edu (Y.H. Cho), junsin@skku.edu (J. Yi).

matrix has gained more focus for easy scalability and control [9,12]. The most important factor behind this embedded fabrication process is the selection of suitable deposition parameters as well as the surrounding dielectric/semiconductor matrix. This vastly affects the electrical conductivity by tuning the energy bandgap based on the growth, size, and distribution density of Si QDs. Thus embedded Si QDs proved to be a promising candidate to form the upper layers for 'all-Si' tandem solar cells with different energy levels, depending on the QDs size and density [11–13]. Previously large number of works were focused on Si QDs embedded in Silicon dioxide (SiO_2) matrix. However, high potential barriers of SiO_2 pulled a drawback in carrier injection efficiency between the QDs [14,15]. Thus other Si dielectric/semiconductor matrix such as Silicon nitride (Si_3N_4), Silicon Carbide (SiC) demonstrated to be the efficient candidates. In this review, we have focused our study on the growth of Si QDs embedded in Si dielectric/semiconductor matrix.

In concern with the growth of Si QDs within the dielectric material, growth parameters play an important role. It was reported that concentration of Si in Si-rich films, high-temperature annealing in inert ambient and controlled pressure of precursor gases result in a qualitative synthesis of Si QDs through the phase separation reaction [16,17]. Phase separation produces Si-QDs embedded in SiO_x ($1 < x < 2$), with multiple defects at the border of Si QDs. These defects disappear on high-temperature annealing. However, an in-situ growth of Si QDs within Si-rich Si_3N_4 dielectrics without any post-deposition annealing was also reported by several research groups [18–21]. Thus the concern over the formation mechanism of QDs is still under debate. Reports suggested room-temperature growth of Si NCs are possible in Plasma enhanced chemical vapor deposition (PECVD) reactor by controlling precursor gas flow and chamber pressure [19]. However, this technique presents a challenge over easy controlling of size and density of Si QDs within the nitride matrix.

The experimental works for the growth of embedded Si QDs in Si dielectric/semiconductor films for photovoltaic applications are reviewed here. For the better understanding of the control over size and distribution of Si QDs, a discussion on different affecting factors is provided. In spite of being the major topic of concern, very few works reported the perfect understanding of the effect of growth parameters on the size and distribution of Si QDs within the Si-based matrix. The main focus of this review is to study the in-depth effects on individual growth parameter during fabrication of Si QDs and their effect on material properties. This review work is organized as follows: In section 2, a theoretical approach for the growth mechanism of Si QDs is described. Different fabrication approaches made in order to obtain the desired Si QDs in the Si-based matrix is discussed in section 3. Individual growth parameters of Si QDs such as Si-based matrix, Si concentration, Precursor gases, doping and annealing parameters are reported in section 4. In section 5, the role of Si QDs in photovoltaic device and finally in section 6, the problem to implement the same as well as an outlook of future progress are conveyed.

2. Theoretical approach and growth mechanism

The growth of QDs within dielectrics is the topic of interest in modern electronics. Various theoretical studies and approaches were made to understand the exact growth mechanism and control it. In order to achieve quantum confinement in Si, at least one dimension has to be restricted to Bohr radius of bulk c-Si which is well understood around 1960s. The superlattice growth for amorphous silicon (a-Si) was first reported in the work of Abeles and Tiedje [22] in 1983. But the theoretical study presented by Brus [23] described the presence of localized dangling bonds in the epitaxial interface of superlattices or quantum well which creates mid-band

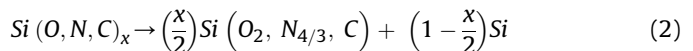
trap states or chemically combine with foreign materials affecting the formation of nanocrystalline. According to his study, the spatial confinement in all three dimensions for nanocrystalline creates distinct energy levels which occupied by electrons following the Pauli Exclusion Principle. In addition, an analytical approximation for the lowest 1S energy state that showed the dependence of bandgap spectra on size and shape of nanocrystalline was explained [23].

A Theoretical study by Cho et al. [24], showed the formation of highly conductive layers by framing true superlattice with wave function overlap of adjacent QDs. The decay rate of wave function was approximated as

$$f(r) = \frac{\exp\left(-\frac{r}{L_d}\right)}{r} \quad (1)$$

where r is the distance between adjacent QDs (measured from the center) and L_d depends on barrier height of the dielectrics in which the dot is embedded. Considering theoretical values, the QDs in SiO_2 and SiC matrix was separated by 1–2 nm and 4 nm respectively for obtaining reasonable wave function overlap and conductivity. Study of Jiang et al. [14], presented the conduction band structure of regular sized Si QDs embedded within the Si dielectric matrix. Anisotropic effective mass of cubic Si QDs was considered to reduce the energy separation between states, which may be favorable for solar cell absorption layer. The proposed model by Ref. [14] showed a feeble effect of QD size on carrier mobility whereas interdot spacing had a drastic effect on mobility as illustrated in Fig. 1a and b. The dot size is 2 nm in all axes (Fig. 1a), whereas the interdot spacing is maintained at 1 nm in all direction for all Si-based matrices (Fig. 1b).

Si QD fabrication in the dielectric matrix is associated with either in-situ growth in nitride matrix or high-temperature growth following the precipitation and phase separation. The theoretical realization of phase separation mechanism was described in the work of Cho et al. [24], which is as follows:



where x represents a positive integer and its value is in-between 1 to 2. A theoretical study on tunneling between quantum dots was presented in the report of Conibeer et al. [15]. Their report presented a mathematical formulation between the barrier heights of surrounding matrix and tunneling probability (T_e) of QDs as follows:

$$T_e = 16 \exp\left\{ -\sqrt{\frac{8m^*}{\hbar^2}} \Delta E^{1/2} \cdot d \right\} \quad (3)$$

The relation clearly illustrates the dependence of T_e on bulk effective mass (m^*), the energy difference between bulk band of Si-based matrix and band formed by QD interaction (ΔE) and spacing between QD (d). Thus the carrier transport between QDs varies depending on barrier height of Si-based matrixes which also predicts that for better tunneling the QDs have to be closest in oxide matrix as compared to carbide matrix.

3. Fabrication technique: growth and deposition

The state of art is the most important stage behind the formation of Si QDs embedded within Si dielectric matrix. Li et al. [25], experimentally described the phase separation of SiO_x ($1 < x < 2$) layers in three steps based on temperature dependence on

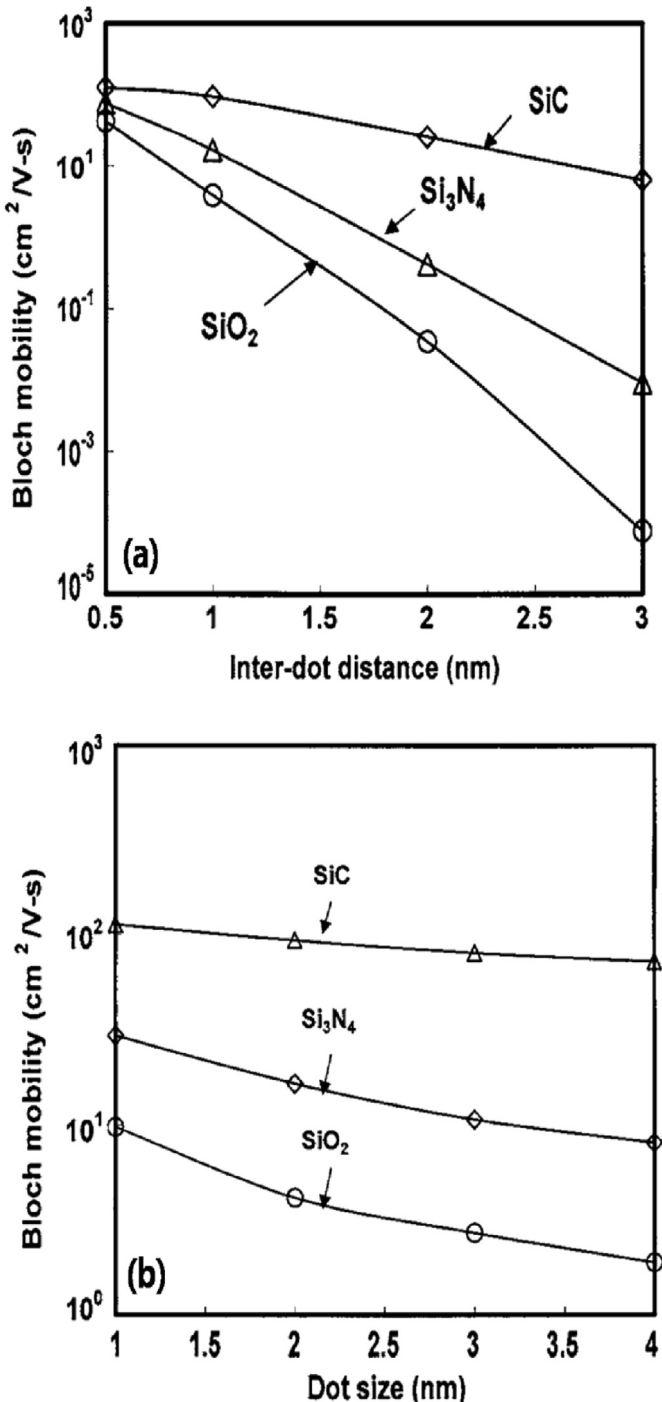


Fig. 1. Theoretical study of Bloch mobility changing with (a) inter-dot distance considering dot size as $2 \times 2 \times 2 \times \text{nm}^3$ and (b) dot size considering interdots distance 1 nm in all direction. Reprinted from Ref. [14], with the permission of AIP publishing.

photoluminescence (PL) and Fourier transform Infrared spectroscopy (FTIR) results. The first step was the reorganization of SiO in SiO₂ matrix detected by Si—O—Si bond stretching and variation of PL intensity. The second step was the precipitation of a-Si cluster detected by the shift in PL peaks and the third step was the crystallization which was observed beyond 900 °C and determined by strong red PL peak. For the synthesis of SiO₂, Si₃N₄ and SiC, industries mostly use the Si precursor gases with other reacting gases in the chemical vapor chamber. Si QDs may be formed within these

matrixes slightly varying the concentration of Si in the silicon-rich layer (SRL) of oxide, nitride or carbide. This change in process parameters may be easily done using the common deposition processes followed by high-temperature annealing. Despite of Si-based matrix, the commonly used synthesis method for the growth of Si QDs includes sputtering [27–38], evaporation [10,26,39,40], chemical vapor deposition (CVD) [17,19,41–56], molecular beam epitaxy (MBE) [57,58], laser ablation [59,60] and high dose ion implantation [61]. Among all the mentioned techniques, sputtering, CVD and reactive beam evaporation are commonly used and suitable for easy formation of Si QDs.

Mostly adopted CVD technique consists of PECVD [41–53], inductively coupled plasma CVD [54], low-pressure CVD (LPCVD) [55] and hot-wire CVD (HW-CVD) [17] due to high throughput and scalable deposition. However, these CVD processes use the cracking of toxic and explosive SiH₄ or other Si precursor gasses that adds up to the disadvantages of CVD process. Control over the flow of this precursor gases along with plasma power and substrate temperature also determines the film uniformity and composition. On the contrary, for co-sputtering technique, the stoichiometry of layers is varied by controlling the deposition rates of Si, Si-based dielectric/semiconductor and doping element. In this case, post-annealing is mandatory for the phase separation growth of QDs within the matrix. Better uniformity and no use of harmful gases turn out to be an advantage for this technique whereas low throughput and high deposition cost are the prominent disadvantages of this technique. Tables 1 and 2 summarize some reported results for the formation of Si QDs in the different matrix using different fabrication techniques, approaches and precursor gases (in case of CVD). The roles of precursor gases behind the formation of Si QDs in the different matrix will be discussed in subsection 4.3.

Apart from diverse deposition technique, size and distribution of Si QDs within the Si-based matrix depend on monolayer and multilayer approach. Depending on the dielectrics, the growth of QDs in monolayer approach is governed by varying deposition rates of elements on the substrate, precursor gas flow rates in CVD chamber with or without post-deposition annealing. In this approach, the uniformity of QD size is the matter of concern. QDs of different size forms within the layer generating a bulk response. Whereas for multilayer approach, QDs are grown by high-temperature post-deposition annealing of multiple alternate layers as formed by SRL sandwiched between stoichiometric Si dielectric layers. Fig. 2 demonstrates the formation of Si QDs within the dielectric matrix in both monolayer and multilayer approach after post-annealing.

4. Growth parameters

The growth of Si QDs depends on the proper growth parameters. Theoretical study presented earlier (in section 2) demonstrated the effect of barrier height along with the distribution of Si QDs plays a vital role in conductivity of QD layer. Thus control over the size and spacing of Si QDs is the matter of interest which hugely depends on the Si-based matrix, the concentration of Si in SRL and approach, the partial pressure of precursor gases, doping element and post-annealing parameters. The effect of each parameter along with previously reported results are discussed briefly in the following subsections.

4.1. Si-based matrix

Si-based matrix plays a vital role in the growth of Si QDs. The electron wave functions for Si, confined in insulating Si dielectric matrix overlap, which results in a shift towards higher energy level. The dielectric/semiconductor matrix determines the process of

Table 1

Tabular representation of sputtering, evaporation and other techniques along with structure, substrate heating, process parameter and post-annealing conditions for growth of Si QDs in different Si dielectrics.

Category	Structure	Targets used	Substrate heating	Process parameter	Post annealing ambient/temperature/time	Ref. No.
Sputtering	SRO monolayer	Si & SiO ₂	No heating	DC power to Si [15–150 W], RF power to SiO ₂ [180 W]	N ₂ , 1100 °C, 1 h (tube)	[27]
		Si & SiO ₂	No heating	RF power to both Si [120 W] & SiO ₂ [60 W]	Ar, 1000–1200 °C, 30s (RTA); 800–1100 °C, 60 min & 1000 °C, 15–180 min (tube)	[28]
	SRO/SiO ₂ multilayer	Si & SiO ₂	–	DC power to Si, RF power to SiO ₂	N ₂ , 1100 °C, 1 h (tube)	[29]
	SRN/Si ₃ N ₄ multilayer	Si & Si ₃ N ₄	No heating	RF power to both	vacuum, 1100 °C, 2 h (tube)	[30]
		Si & Si ₃ N ₄	–	DC power to Si [6 W], RF power to Si ₃ N ₄ [50 W]	N ₂ , 900–1100 °C, 1 h (tube)	[31]
	Monolayer SRC	Si & SiC	No heating	RF power to both	N ₂ , 1100 °C, 1 h (tube) or 1100 °C, 1 h (RTA)	[32]
	SRC/SiC multilayer	Si & SiC	No heating	DC power to SiC [6 W], RF power to Si [50 W]	N ₂ , 800–1100 °C, 9–25 min (tube)	[33]
	P doped SRO/SiO ₂ multilayer	Si, SiO ₂ & P ₂ O ₅	No heating	–	–, 1100 °C, 1 h	[34]
	B doped SRO/SiO ₂ multilayer	Si, SiO ₂ & B ₂ O ₃	–	RF power to all target, B target [100 W]	N ₂ , 1100 °C, 30 min (tube)	[35]
		Si, SiO ₂ & B target	–	RF power to all target, B target [0–50 W]	N ₂ , 1100 °C, 1 h (tube)	[36]
Thermal Evaporation	Sb doped Si ₃ N ₄ monolayer	Si, Si ₃ N ₄ & Sb target	–	RF power to all target	N ₂ , 1100 °C, 1 h (tube)	[37]
	SRO monolayer	Si & SiO ₂	–	RF power to all target	–, 300–1200 °C, 30min–2h	[38]
	Sn doped SRO thin film	single crystal Si, SiO ₂ & Sn powder	150 °C	SiO ₂ : Si powder = 3:1, mixed with Sn powder (0.01 fraction of Si)	Ar, 400–1100 °C, 30min	[39]
Reactive Evaporation	SiO _x /SiO ₂ super lattice	SiO powder	100 °C	evaporation of SiO powders in O ₂ atmosphere	N ₂ , 1100 °C, 1 h (tube)	[10]
e-beam Evaporation	SRN monolayer	Si source,	100 °C	Si evaporated in N ₂ ambient	10 ⁻⁸ Torr, 950 °C, 1–20 h (tube)	[26]
	SiO/Si multilayer	Si & SiO source	–	alternate evaporation of SiO & Si via e-beam	N ₂ , 1100 °C, 1 h (tube)	[40]
Molecular beam epitaxy	SiO ₂ /Si multilayer	–	No heating	six period Si/SiO ₂ super lattice was made	No annealing	[57]
	B doped Si layer	–	420 °C, 700 °C	Either zero or negative bias applied to the substrate	Ar, 200–500 °C, 15 min (tube)	[58]
Laser ablation	Si NC on graphite	Si target	–	Si NC grown in basal plane of graphite	–, 500–600 °C, 5 min	[59]
Pulsed laser ablation	SRO monolayer	Si target, O ₂ gas	–	Si plasma in O ₂ atmosphere deposited on substrate	N ₂ , 1000–1200 °C, 10–20min (tube)	[60]
Ion implantation	SRO monolayer	Si ⁺ ion source	–	Dry thermal oxide grown on substrate, Si ⁺ ion implanted at 50 keV	N ₂ , 1100 °C, 1 h (tube)	[61]

Table 2

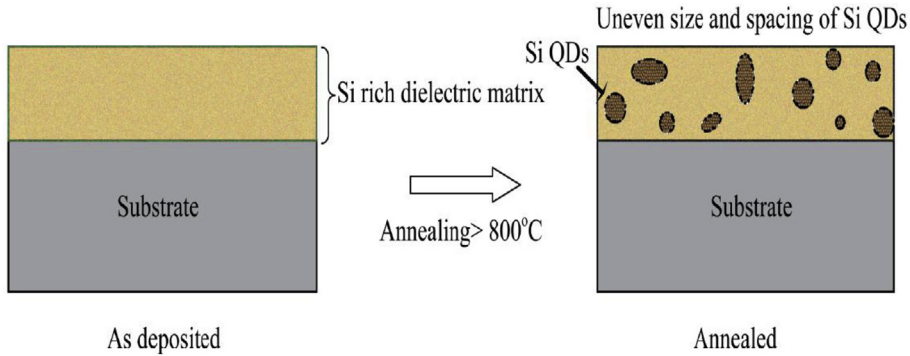
Tabular representation of different CVD techniques along with structure, substrate heating, precursor gas and post-annealing conditions for growth of Si QDs in different Si dielectrics.

Category	Structure	Precursor gases	Power/Power density	Substrate heating	Post-annealing ambient/temperature/time	Ref. No.
PECVD	SRO monolayer	SiH ₄ & N ₂ O	–	400 °C	–, 1180 °C, –	[41]
		SiH ₄ , Ar & N ₂ O	–	–	Ar, 1000–1250 °C, 30 min	[42]
	SRO/SiO ₂ multilayer	SiH ₄ , H ₂ & N ₂ O	40 W	200 °C	N ₂ & Ar, 1100 °C, 1 h	[43]
	SRN monolayer	SiH ₄ , NH ₃ & He	5 W	300 °C	N ₂ , 1100 °C, 1 h	[44]
		SiH ₄ , NH ₃ & N ₂	10 W	300 °C	No annealing	[19]
		SiH ₄ & N ₂	6 W	300 °C	No annealing	[45]
	SRN/Si ₃ N ₄ multilayer	SiH ₄ , NH ₃ & N ₂	15 W	375 °C	N ₂ , 1150 °C, 1 h; H ₂ , 500 & 700 °C, 1 h (some samples)	[46]
		SiH ₄ , NH ₃ & Ar	–	400 °C	N ₂ , 600–1150 °C, 2 h	[47]
	SRC monolayer	SiH ₄ , CH ₄ & Ar	–	250 °C	N ₂ , 500–1100 °C, 30 min	[48]
		SiH ₄ , CH ₄ & H ₂	160 mW/cm ²	200 °C	N ₂ , 750–1200 °C, 30 min	[49]
SRC/SiC multilayer	SiH ₄ , CH ₄ , H ₂ & Ar	0.1 W/cm ²	250 °C	N ₂ , 1100 °C, 30 min	[50]	
	B doped SiO _x thin-film	SiH ₄ , B ₂ H ₆ , CO ₂ & Ar	100 W	200 °C	No annealing	[51]
	SRON:P/SiO ₂ multilayers	SiH ₄ , PH ₃ , & Ar	–	–	N ₂ , 1150 °C, 1 h	[52]
	SRC monolayer	SiH ₄ , CH ₄ & H ₂	14 W	150 °C	No annealing	[53]
	SRO/SiO ₂ multilayer	SiH ₄ , Ar & N ₂ O	–	250 °C	N ₂ , 900 °C, 1 h	[54]
LPCVD	Si/Si _x multilayer	SiH ₄ Cl ₂ & H ₂	N.A.	–	N ₂ & H ₂ , 1000 °C, 1 h	[55]
HWCVD	Si/SRN multilayer	SiH ₄ & NH ₃	N.A.	250 °C	Ar, 800–950 °C, 30 min	[17]
Cat-CVD	SRN monolayer	SiH ₄ , NH ₃ & H ₂	N.A.	200 °C	No annealing	[56]

crystallization and the interface between the Si-QDs with its surroundings. As a result, it plays a crucial role in determining the optical properties of the Si QDs embedded photovoltaic devices that enhance the capacity of absorbing high energy photons from

solar radiation. Besides the conductivity of the device, depends enormously on the distribution of Si QDs as well as the surrounding matrix. The carrier mobility through the Si-based matrix depends on its barrier height and Si QD superlattices which were discussed

Mono-layer approach



Multi-layer approach

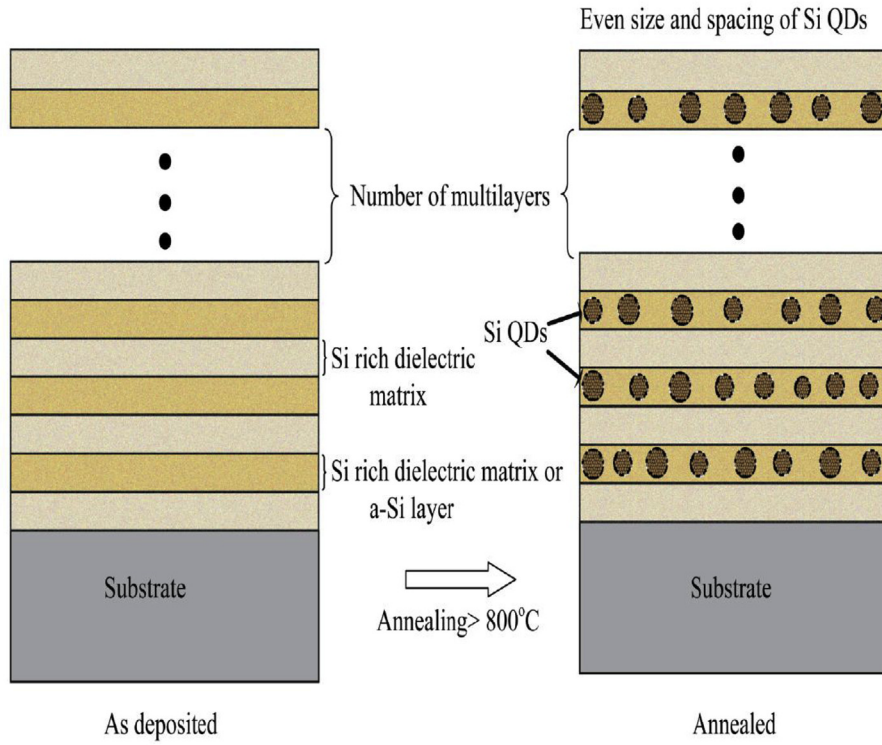


Fig. 2. Schematic diagram showing mono-layer and multi-layer approach for the formation of Si QDs embedded in Si dielectric matrix on post-annealing beyond 800 °C. Adapted from Ref. [24].

based on the theoretical approach by Jiang et al. [14]. (in section 2). Wide bandgap Si QDs with small inter dots spacing increases the range of photon absorption along with the increase in minority carrier lifetime that determines the carrier density in solar cell absorber. This, as a result, determines the short circuit current and open circuit voltage through quasi-Fermi level splitting.

Many past studies were conducted for the growth of Si QDs in the oxide matrix. But Zacharias et al. [10], first reported the growth of size and distribution controlled Si QDs in SiO_2 matrix. They reported the ordered arrangement of Si NCs by phase separation and high-temperature annealing of SiO/SiO_2 superlattice. Si NCs diameters of 3.8, 2.5 and 2.0 nm keeping uniform distribution density were investigated with a detailed analysis through transmission electron microscope (TEM) (shown in Fig. 3) and their PL for interfacial defects (shown in Fig. 4). Yi et al. [62], reported high distribution density (up to $10^{19}/\text{cm}^3$) growth of Si-NCs with the

crystal diameter up to 2 nm. This work demonstrated the control of Si NCs size by varying the thickness of amorphous matrix from 2 to 7 nm. An interesting fact described by the same author that a bulk property was demonstrated for SiO layer above 5 nm of thickness. However, the high barrier height of Si/SiO₂ superlattices makes charge carrier transport difficult through the Si-QD networks. This created a concern for the mobility of the device where Si QDs embedded in SiN_x and SiC system comes into the role.

Switching to Si/SiN_x and Si/SiC system with a barrier height of 1.9 eV and 0.5 eV (shown in Fig. 5) seems to be more feasible. This increases the probability of electron tunneling through the barrier, which increases mobility as compared to SiO_2 [14]. The density of Si QDs is more in pure Si_3N_4 as found in other dielectric material [63]. In addition, a low interfacial defect with high PL intensity at shorter wavelengths is observed for Si QDs in SiN_x matrix. Silicon-rich nitride (SRN) and multilayer of a-Si/SiN_x structures are mostly

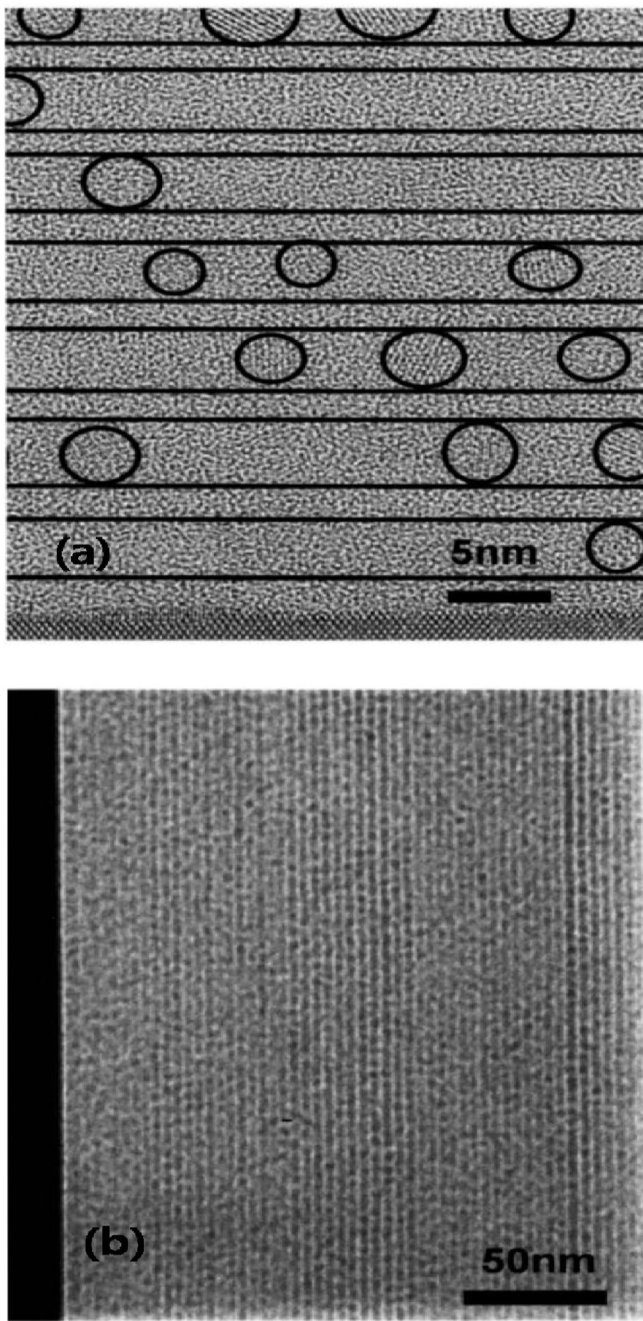


Fig. 3. Cross-sectional TEM images of SiO/SiO₂ superlattices: (a) Formation of Si QDs after annealing with a perfect separation by thin oxide shell. (b) Image ~2 nm SiO layers after annealing. Reprinted from Ref. [10], with the permission of AIP publishing.

studied for the growth of Si QD in SiN_x. Park et al. [45] reported the formation of 1.4–2.4 nm a-Si QDs within the Si₃N₄ matrix which they confirmed by a shift in the PL emission peaks from 2.0 to 2.76 eV. Other research groups also reported the formation of a-Si QDs within as deposited SiN_x films without properly controlled growth of QDs [28,31,44]. The study for a-Si/SiN_x multilayer started with the formation of multi-quantum well that showed an intense visible PL peak at ~2 eV for 4 nm well thickness [64]. However, proper study on the controlled growth of Si NCs in a-SiN_x/a-Si:H/a-SiN_x structure was first reported by Zhang et al. [65]. They demonstrated that the nitride barrier layers determine the size and shape of Si NCs within the system leading to the formation of disc-shaped crystals. The works of Panchal et al. [17] and So et al. [31]

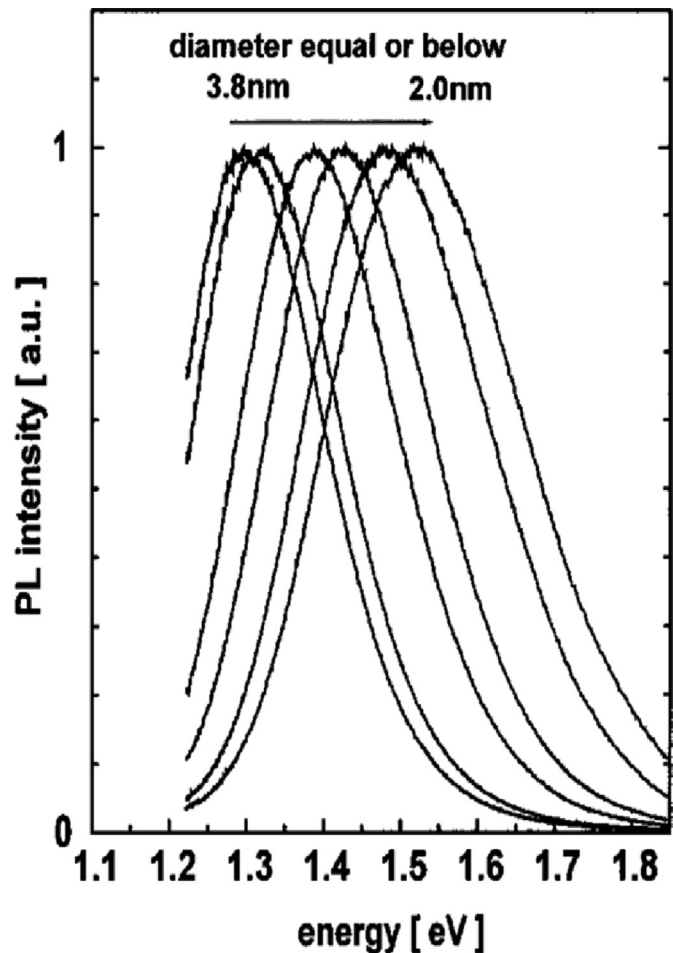


Fig. 4. PL spectra showing a blue shift with the decrease in Si QDs size within the SiO₂ dielectric. Reprinted from Ref. [10], with the permission of AIP publishing.

presented the formation of Si NCs through SRN/SiN_x multilayer approach. PL results presented by So et al. [31] showed a shift from 1.65 eV to 1.75 eV by an increase in temperature from 900 to 1100 °C which is attributed to better passivation of Si QDs, despite their diameter size. The formation of Si QDs within SRC matrix was studied by Künle et al. [66]. The formation of QDs in both SRC mono-layer, as well as SRC/SiC multilayer matrix was investigated by the same authors. Si NCs from 1 nm to 13 nm was observed to form in monolayer SRC whereas the formation of Si NCs as well as SiC NCs was observed for multilayer approach. Low enthalpy of Si–C bonds as compared to oxide and nitride bonds make the formation of Si-QDs much more complex resulting in dissolving of SRC/SiC multilayer structure forming Si QDs, SiC QDs and a-Si with annealing 1100 °C temperature [66]. Thus for proper growth of NCs in SiC matrix control over annealing as well as passivation of bonds is necessary.

4.2. Role of Si concentration in Si-rich layer

The concentration of Si in SRL is one of the most investigated factors to determine the structural properties of embedded Si QDs. The chemical stoichiometry of O/Si, N/Si and C/Si affect significantly the size distribution and spacing of Si QDs [67]. Controlling the sputter rate and precursor gas flow, the content of Si may be controlled in SRL. Earlier studies suggest the formation of Si QDs by high-temperature annealing of Silicon rich oxide, nitride, carbide and oxynitride (SRO, SRN, SRC and SRON) mono-layer with a broad

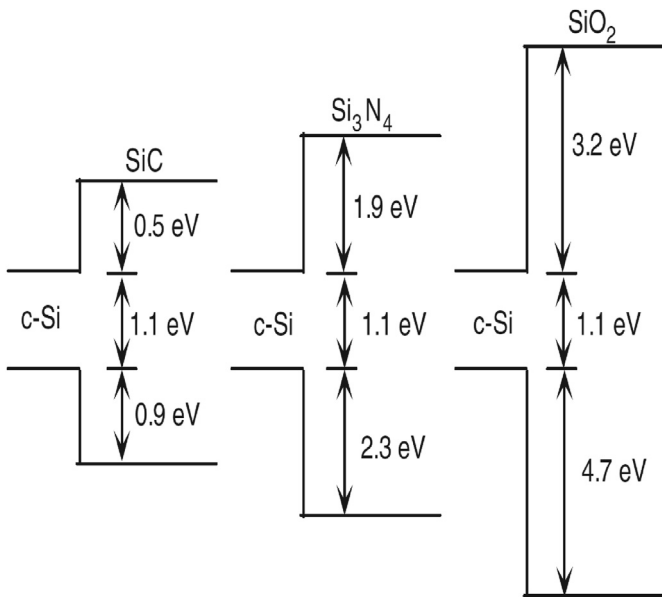


Fig. 5. Bulk band offsets between Silicon dielectrics and crystalline silicon. Reprinted from Ref. [15], with the permission from Elsevier.

range of size and unorganized distribution of QDs. However, in order to produce size controlled and well distributed QDs using mono-layer approach, appropriate thickness and favorable annealing conditions are required. Kahler et al. [68]. reported the formation of 3–4 nm of the diameter of Si QDs from an SRO monolayer with the stoichiometric value of x in the range of 1.2–1.6. Their study presented a blue shift in PL peaks with a decrease in intensity which is attributed to decrease either in the absorption cross-section or the distribution density of Si NCs. Huang et al. [69]. showed the dependence of O/Si ratio on Si NCs growth through SRO mono-layer approach, where with the increase in O/Si ratio phase separation gets delayed resulting the decrease in crystallinity fraction from 39.4% to 22.7%.

In order to restrain the size of QDs, a multilayer approach of SRO/SiO₂ was proposed by Zacharias et al. [10]. For the multilayer approach, size of Si QDs may be controlled in the direction perpendicular to film by the thickness of SRO layer, which is sandwiched between two consecutive SiO₂ layers. The high-resolution image of TEM clearly indicated the size distribution of Si NCs which were dependent on the thickness of the SRO layer. Higher distributions of NCs are also observed for the sample with ~2 nm buffer oxide layer, which was strongly supported by the blue shift, with no decrease in intensity of PL peaks shown in Figs. 3 and 4. Study of Cho et al. [24]. showed the formation of spherical Si QDs with the diameter similar to the thickness of the SRO layer. Yi et al. [62]. reported the control over QDs size and density of the QDs, which may be adjusted through the stoichiometry of SRO layer. On increasing the value of x (mole fraction) of SiO_x, the intensity of PL peaks increased with small blue shift indicating the enhancement of Si NCs with a small decrease in size as shown in Fig. 6. Hao et al. [29]. also reported the same stoichiometric observation on the distribution density of Si QDs in SRO from the Grazing incidence x-ray diffraction (GIXRD) peaks.

The stoichiometric growth of Si QDs in silicon nitride dielectric matrix, mono-layer as well as SiN_x/Si₃N₄ multilayer approaches are also reported elsewhere [30,31,44–47]. Nguyen et al. [30]. reported the formation of Si NCs within the amorphous matrix may be maneuvered by controlling the Si content percentage in SRN. The high-resolution TEM (HRTEM) images presented in their report confirms the NCs formation for 62% and 47% Si content whereas no

NCs are observed for 40% Si sample. Another research group also reported a blue shift in the PL peaks which was ascribed to less quantum confinement effect due to the decrease in size (10–3 nm) of Si QDs in SRN [70]. This decrease in size was due to less excess Si content within the SRN layer. For the study of the organized size and inter dots spacing between QDs, multilayer approach using a-Si/SiN_x is adopted in the works by Panchal et al. [17,71]. Due to size controlled Si QDs, cell structure presented in Ref. [71] showed a promising I–V characteristic. The formation of Si QDs in SiC matrix, with SRC/SiC multilayer approach, was also studied [50,66]. Künle et al. [66]. reported the variation of crystallization temperature with the variation of SiC stoichiometry. Authors reported that in SRC/SiC multilayer approach, the growth of Si NCs takes place at 900 °C for Si_{0.9}C_{0.1} and 1000 °C for SiC. They also reported the crystallization of both the layers starts at 1000 °C for Si_{0.7}C_{0.3}. Reports of Song et al. [72]. showed that the multilayers behavior were dependent on SiC stoichiometry based on carbon content. Results of Cho et al. [73]. was also in good agreement with others, which demonstrated Si QDs embedded in SiC matrix as a promising candidate for ‘all-Si’ tandem solar cell. Although multilayer approach is mostly adopted, the merging probability of Si QDs to form polycrystalline Si during annealing is high, which results in a decrease in luminescence efficiency.

4.3. Partial pressure of precursor gases

The fundamental behind the formation of silicon dielectric/semiconductor matrix is the chemical recombination of precursor

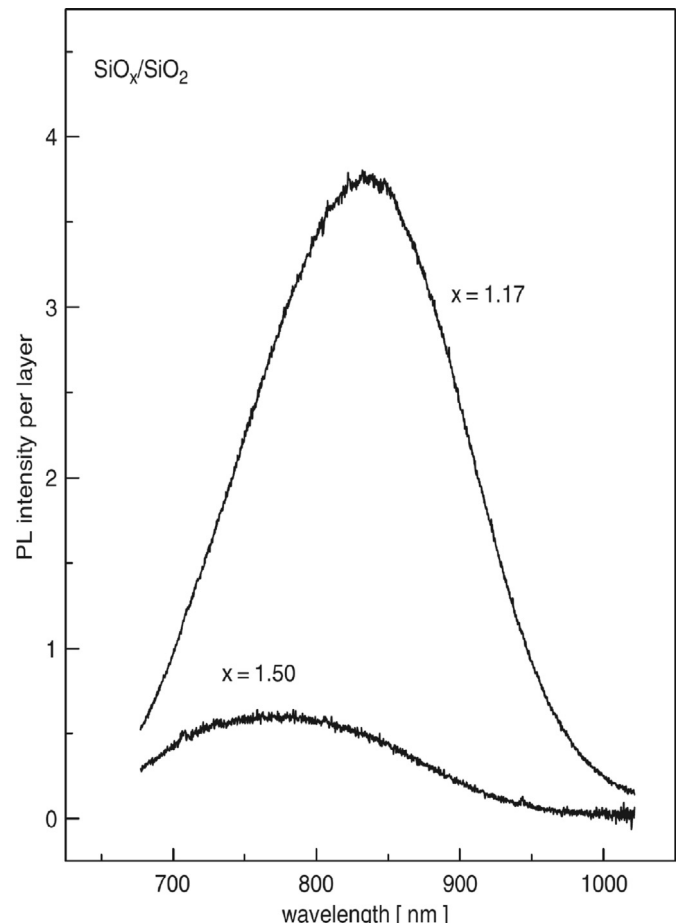


Fig. 6. PL spectra of annealed SiO_x/SiO₂ superlattices with varying the stoichiometry of SiO_x. Reprinted from Ref. [62], with the permission from Elsevier.

gases inside the CVD chamber. SiH₄ is widely used as a precursor gas for Si accompanied by N₂O or O₂ for SRO, NH₃ for SRN and CH₄ for SRC, respectively. However, the introduction of dopant precursor gases with a perfect flow ratio also control the doping state of the Si NCs. In order to achieve the stoichiometric composition, the flow rates of gases are required to control and studies accordingly.

In case of the formation of SRO, the flow of SiH₄ gas within O₂ environment was reported earlier [74,75]. But this forms Si—O—Si bond with low bond angles that easily break during the process and give rise to defect centers. In order to avoid the defect factor, O₂ flow is highly diluted with Ar by a factor of approximately 1:1000 [75]. To form a defect-free SiO₂ layer, higher oxygen content N₂O gas as a precursor was reported. Safe and Low activation energy of N₂O makes advantageous to the process whereas incorporation of nitrogen and hydrogen as impurity adds up as disadvantage [67,76]. Presence of nitrogen reduces the absorption efficiency, resulting in the decrease in the mobility of silicon in SRO as compared to nitrogen-free layers. It affects, the phase separation increasing the crystallization temperature. Studies suggest the formation of high-density Si NCs with the variation of SRO stoichiometry by controlling the flow ratio of SiH₄/N₂O [41]. Tuning of N in SRO layer is the scope to control the size of Si NCs in oxynitride matrix as reported by Hartel et al. [67]. To obtain the quality Si NCs as observed from PL intensity, the variation of gas flow rate has a major role [67].

Table 2 shows several reports of Si NC formation within Si₃N₄ matrix using SiH₄ and NH₃ gas as a precursor for CVD technique. Barbé et al. [44] showed that the change in flow rate of SiH₄ and NH₃, the composition of Si changes within the dielectric matrix that controls the crystallization of Si NCs. They calculated the change of molar fraction with the change in NH₃/SiH₄ ratio which is shown in **Table 3**. Si NCs were agglomerated as noticed for high Si content film as compared to low Si content films, which was evidenced from XPS peaks of post-annealing Si components for x = 0.7. Lee et al. [56], demonstrated the formation of Si NCs of size 3.5 nm–5 nm by varying NH₃/SiH₄ mixture ratio. The PL peaks as observed in their result continuously shifted from 710 nm to 510 nm which indicates the change in NCs size during 200 °C processing temperature. In order to grow Si QDs embedded in SiC matrix, CH₄ is mostly used as a precursor in the PECVD chamber with a controlled plasma power and substrate temperature as specified in **Table 2** [48–50,53]. To study the effect of SiC stoichiometry on the growth of QDs, Summonte et al. [77] varied the Si atomic fraction from 0.55 to 0.75 by monitoring the flow rate of SiH₄ from 1.6 to 11.4 sccm keeping the flow of CH₄ and H₂ as constant at 70 and 10 sccm respectively. Use of monomethylsilane (MMS) as a precursor gas for carbon source was also reported in the work of Kurokawa et al. [78]. Control over the precursor gas ratio gave the access to control Si content in the SRLs which affect the crystallinity and formation of Si QDs. Introduction of B₂H₆ [51] and PH₃ [52] in the PECVD chamber acted as the precursor gases for B and P doping of Si QDs respectively. The doping profile of the Si QDs

was controlled through the flow ratio of the dopant gases with the SiH₄. Apart from that, authors of reference [51] also observed that Ar flow in the PECVD chamber had an impact on the phase transition of Si and size of the QDs.

4.4. Doping element

Doping of Si QDs for photovoltaic application is also an important scenario for improving the conductivity by increasing carrier concentration. The concentration of dopants also control the interfacial defects that enhance the optical properties of NCs. Previous reports showed that doping kinetics vary drastically within the self-purified nanocrystals which results in large impurity formation energy [79–81]. As a result, quantitative characterization of dopant element within the QD structure becomes tricky [52]. Apart from this difficulties, injection of impurities like boron (B) [35,36,51,82–84], phosphorus (P) [34,52,85–88], and antimony (Sb) [37] reported to have a desired change in the conductivity as well as interface defects of the doped films. Incorporation of doping elements are done only changing the O/Si ratio with the dopant concentration in SRL by commonly followed sputtering or CVD technique [34,36,89,90].

Kanzawa et al. [35] first reported a successful boron doping of Si NCs by RF co-sputtering of Si, SiO₂ and B₂O₃ and confirmed through the Raman study, as presented in their work. However, a proper understanding on the work of dopant atoms in upgrading the optoelectrical properties of confined Si NCs in the dielectric matrix was not obtained till 1998. Fujii et al. [84], first reported atypical temperature dependence and quenching of exciton PL with an increase in B concentration. This typical behavior was attributed to Auger recombination among free hole and the exciton as-generated from the neutral B state. A similar reduction of exciton PL due to heavy P doping was also reported by Mimura et al. [87]. Infrared absorption spectroscopy demonstrated the generation of excess electrons that non-radially recombined with photo-excited excitons, which results reduced PL. But an increase in PL efficiency was observed by Fujii et al. [88] when the Si NCs were doped with P dopants. This result ascribed that an increase in P concentration decreased the interfacial defects within the dielectric rather than substituting Si atom. A similar defect passivation and enhancement of PL result were further showed by Nomoto et al. [52], where they analyzed P distribution within the Si NCs for 2 nm diameter. Whereas in other work, Nomoto et al. [89], studied the distribution of B and P atoms within the Si NCs. The atomic probe tomography (APT) analysis showed the formation of B and P rich layer near the Si NCs whereas the formation of B–P clusters was confirmed for co-doped Si NCs. These clusters act as a donor and collector level, quenching the PL energy from co-doped Si NCs. In addition, several noteworthy studies were reported to enhance the electrical property of Si NCs due to doping. Hao et al. [34], confirmed the doping of phosphorus in the Si QDs with a drastic change in the resistivity of the samples. A notable change in the phase separation in the SRL and Si crystallization is observed. In another work of Hao et al. [90], reduction of resistivity by six orders is noted for boron doping in the Si QDs, which is confirmed by the formation of B–Si bond in XPS results. In this case, suppression in Si crystallization is observed with little influence on the QDs size. Zhang et al. [91], demonstrated KrF pulsed laser annealing as a substitute of furnace annealing that can increase the concentration of electrically active dopants (both P and B) without significant change in Si NCs size. The authors concluded that high energy photons activate the interstitial dopants within the Si NCs which can be clearly observed from the electrical studies presented in their report.

Improved electrical conductivity was also reported in the work of So et al. [37] by effectively doping Sb in Si NC embedded in Si₃N₄

Table 3

Variation of Si content ratio x with the variation of precursor gas flow ratio y as reported in Ref. [44]. Reprinted from Ref. [44], with the permission from IOP science.

Sample	y = $\frac{\text{NH}_3}{\text{SiH}_4}$	NH ₃ (sccm)	SiH ₄ (sccm)	He (sccm)	x = $\frac{\text{N}}{\text{Si}}$
y0	0	0	36	35	0
y0.7	0.7	24	36	45	0.47
y1	1	30	30	40	0.67
y1.3	1.3	36	45	64	0.82
y1.7	1.7	36	60	64	0.90
y3.3	3.3	18	60	52	1.12
y5	5	12	60	48	1.26
y10	10	60	6	44	1.33

matrix. Si NCs of diameter 5–7 nm with interspacing of 2–4 nm is observed to improve the conductivity by the six orders of magnitude. Furthermore, different studies with different doping materials were reported with their effects on the crystallization for Si NCs formation. Yoon [92] reported the effect of nickel (Ni) doping on the formation of Si NCs as the concentration of Ni doping hugely affect the process parameters of Si NCs formation. Low Ni concentration accelerated the Si NCs formation, whereas at high Ni concentration NiSi₂ NCs were formed. Similar results were also reported for tin (Sn) doped Si NC samples with the formation of smaller size of Si NCs as compared to undoped samples [39]. Thus control over the dopant concentration has a major effect on the formation and structural parameters of Si NCs.

4.5. Post-deposition annealing parameters

Growth of Si QDs within the dielectric matrix is governed very much by post-deposition annealing temperature and time. In high temperature, Si starts to precipitate within the SRL or a-Si crystallizes in-between the dielectric matrix to form Si NCs. Depending on these interlayer types, annealing time also varies. Si QDs were formed from SRL interlayer after long thermal annealing (LTA), whereas the same was formed from a-Si layer using rapid thermal annealing (RTA) [93]. As compared to bulk crystallization, this process involves crystalline seed creation accompanied by the influence of dielectric interface, surrounding strain, defects at the

grain surface.

Nesbit [16] first studied the growth of Si NCs in silicon-rich SiO₂ films for varying annealing temperature between 700 and 1100 °C. He reported the formation of a substantial amount of Si NCs in between 800 and 950 °C. Later on, Zacharias and Streitenberger [94] found that crystallization temperature (T_c) depends exponentially with oxide interface. This exponential relation was empirically fitted as follows:

$$T_c = T_{ac} + (T_{melt} - T_{ac})e^{-\frac{d}{C}} \quad (4)$$

where T_{melt} represents the melting temperature of bulk crystalline Si, T_{ac} is the crystallization temperature of bulk a-Si film, d is the real thickness of a-Si film and C is the fitting constant. This mathematical expression does not depend on the material properties of the surrounding dielectric matrixes and thus holds for all sort of dielectric.

However, the studies reported the formation of Si QDs within SiO₂ matrix is accompanied by high annealing temperature between 1000 and 1200 °C as compared to SiN_x matrix (800–1000 °C) [93,95,96]. In case of SiC matrix, Si QDs form in SRC layer at 800 °C as reported by Küne et al. [50]. The FTIR peaks reported in their work showed that a broad Si bonding peak (with Si–H and C–H peaks) that started to get narrow to a sharp Si–C bond signifying the formation of Si QDs on annealing from 800 °C and beyond as shown in Fig. 7. Whereas, others have reported the formation of

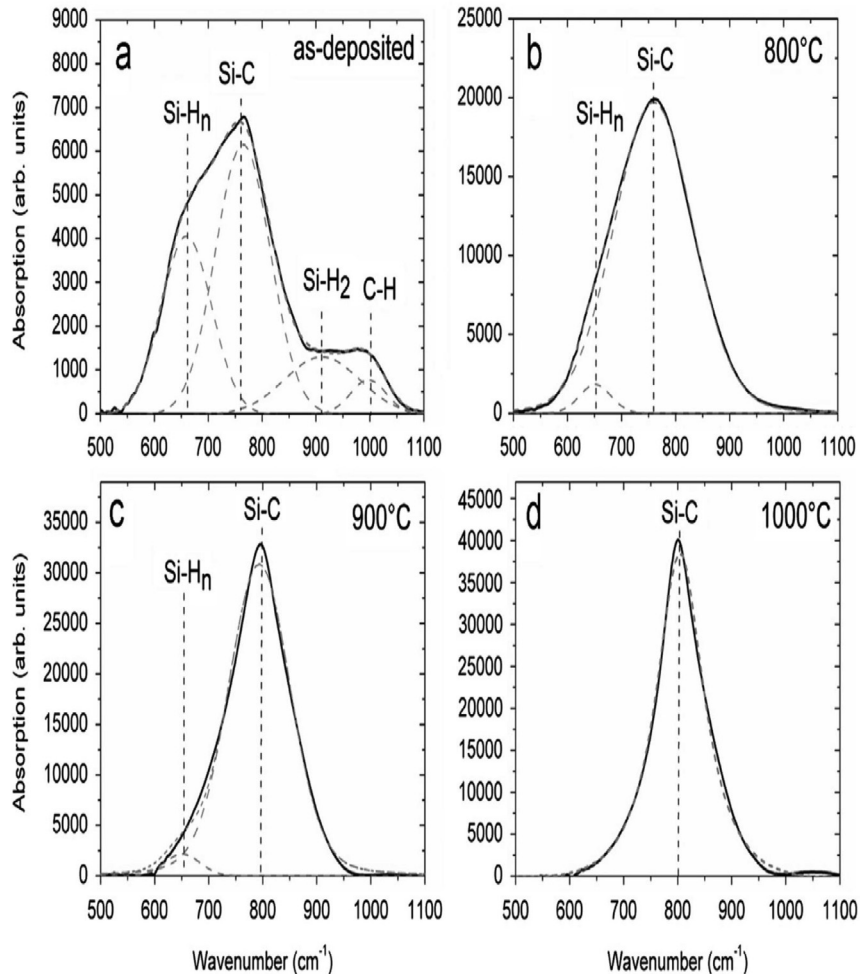


Fig. 7. FTIR spectra of Si_{1-x}C_x/SiC superlattices of (a) as-deposited film and annealed film at (b) 800 °C, (c) 900 °C and (d) 1000 °C respectively. Reprinted from Ref. [50], with the permission from Elsevier.

NCs with the crystallization of SiC in between 900 and 1000 °C depending on the stoichiometry of the SRL [32,33,48–50]. The annealing temperature, time and ambiance reported for different approach of Si QDs formation is summarized in Tables 1 and 2. Apart from post-deposition annealing, the atmosphere inside the annealing furnace also influenced the structural characteristics of the Si QDs. Studies were conducted on the variation of annealing atmosphere and its effect on the structure of the films [43]. Literature suggests annealing in N₂ atmosphere reduces the size of the Si QDs due to the decrease in Si diffusion within the matrix in the presence of excess N₂ [97,98]. A similar scenario was reported by Wang et al. [43], where low distribution density of Si QDs was observed for N₂ annealing as compared to Ar annealing. In order to obtain better crystallinity, RTA proved to be promising as compared to tube furnace post-deposition annealing [32]. However, the author of reference [98] reported no effect of RTA or tube furnace annealing on the formation of Si QDs in SiO_x/SiO₂ matrix. In case of RTA, Rapid temperature ramping may induce a residual stress on the layers that may affect the QDs growth whereas tube furnace annealing markedly reduce the stress on the layers.

5. Ongoing trends in solar cell application

As a promising candidate for the third generation photovoltaic device, the implementation of Si QD has already raised an attention. In order to achieve beyond the Shockley–Queisser limit, various theoretical approaches were proposed by Green [99] and Conibeer [100]. With the goal to achieve the limit, various photovoltaic devices were reported using Si QD structure. Starting from single layer to tandem layer approach using p-type and n-type Si QDs on n-type and p-type c-Si substrate respectively were used to improve solar cell parameters [71,101–104]. On implementing as a photovoltaic device, it is expected to achieve high open circuit voltage (V_{oc}) from a QD device. Despite having a larger bandgap of Si QDs as absorber layers, a poor carrier transport between the QDs, small active cell area and the mismatch between the layer potentials add up to the worst performance of the device. As a result, low V_{oc} with a low fill factor (FF) and efficiency was obtained.

As compared to monolayer Si QD solar cell, promising solar parameters are obtained from tandem structured devices. Uneven size distribution and spacing between inter dots hinders the carrier mobility of monolayer devices. Considering the Si QD stack structured device, Hong et al. [102], reported the highest efficiency of 13.4% from p-type Si QDs/n-type c-Si device, which is shown in Fig. 8. Heavily boron doped emitter cell produced a V_{oc} of 525 mV and short circuit current density (J_{sc}) of 33.7 mA/cm² with 78.5% FF. P-type Si QDs/n-type c-Si heterojunction devices produced a V_{oc} of 463 mV with a FF of 53% was reported by Song et al. [104]. Panchal et al. [71], reported the absorber layer of SiN_x/a-Si/SiN_x stack structured solar cell with poor V_{oc} of 2 mV which is observed to improve beyond 70 mV due to annealing and H₂-passivation. In order to study the photovoltaic effect of Si QDs, Perez-Wurfl et al. [105] fabricated p-i-n layer on foreign (quartz) substrate using B and P as for p- and n-type respectively. High-temperature annealing of the p-i-n structure produced a V_{oc} of 373 mV which further improved by the same research group to 492 mV V_{oc} and 0.02 mA/cm² short-circuit current [13]. A similar n-i-p structure fabricated on quartz substrate was studied by Yamada et al. [103], which produced V_{oc} of 518 mV with FF of 51%. Löper et al. [7], reported a V_{oc} of 282 mV which was obtained from a p-i-n structure fabricated on a membrane-based substrate. Similar approach of p-i-n structure on membrane was performed by López-Vidrier et al. [106] in order to study the effect of Si NC/SiC multilayer on photovoltaic properties. 40 times increment in J_{sc} was observed with tandem 4

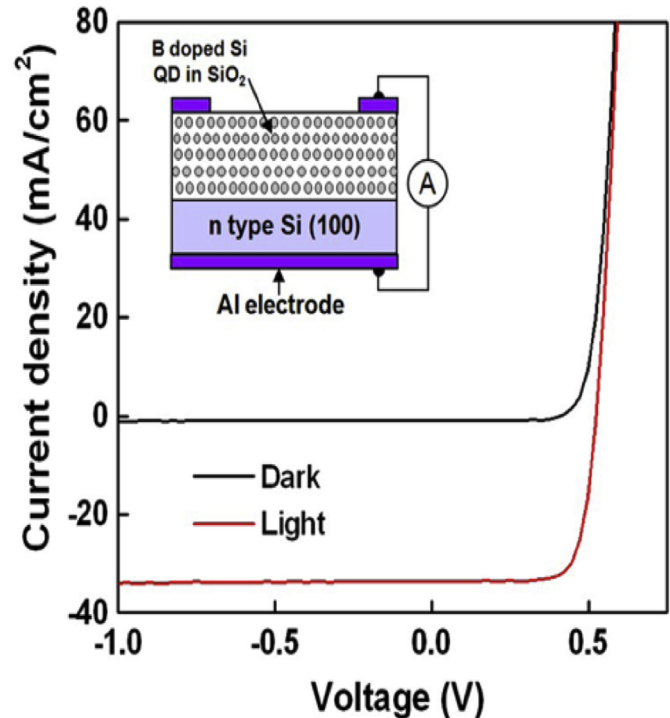


Fig. 8. Dark and light Current–voltage (IV) characteristics of B doped Si QD heterojunction solar cell. The schematic diagram of the cell connection is also shown. Reprinted from Ref. [102], with the permission from IOP science.

layered structure ($V_{oc} = 180$ mV) as compared to monolayer SiC ($V_{oc} = 260$ mV). A brief summary on solar cell parameters for Si NC solar cells as reported by various research groups are shown in Table 4. The promising approaches as mentioned in Table 4 through the timeline has not only produced a fruitful result but also opened a doorway for the practical realization on a new concept to achieve better solar cell parameters.

The realization of Si QD based ‘all-Si’ tandem solar cell may achieve beyond the expected to form a highly efficient solar cell. Very few works have been reported with the practical realization of this concept. Janz et al. [107], reported the formation of first Si QD/c-Si-based tandem solar cell device with the concept of formation of ‘all-Si’ tandem solar cell. Si NC top cells were interconnected with the c-Si wafer that forms the bottom layer of the bifacial cell which recorded to produce V_{oc} of 978 mV from the front side of the cell. The major issue with the formation of ‘all-Si’ tandem solar cell is: (I) improper charge transfer between the QDs of individual cells, (II) unwanted tunnel junctions at interconnects of the cells, and (III) mismatch of the electrical properties of individual cells that leads to poor performance. Other concepts include the formation of hot carrier solar cells using Si QD layer as a sensitive hot carrier selector [100,108]. The Si QD layers act as a double barrier resonant tunnel that allows passage of selective carriers with similar longitudinal energy [108]. As a result, a delay in the cooling of hot carriers may be occurred before getting collected.

6. Conclusion

In this review work, the different combination for the synthesis of Si QDs and its capability to develop a highly efficient solar cell is discussed in-detail. Tuning the size of Si in quantum level, the band gap of the QDs may be tuned to overcome the Shockley–Queisser limit for c-Si solar cell. The control parameters to fabricate Si QD structures within the Si-based dielectric matrix are reviewed here.

Table 4

Tabular summarization of the photovoltaic properties of Si NCs solar cells with respect to fabrication techniques.

Fabrication Technique	Cell structure	Voc (mV)	J _{sc} (mA/cm ²)	FF %	η (%)	Ref. No.
PECVD	p-i-n device on membrane	282	0.339	—	—	[7]
Sputtering	p-i-n device on quartz	492	0.02	—	—	[13]
HWCVD	p-i-n structure on n-type C–Si substrate	70	I _{sc} = 843 nA	—	—	[71]
Sputtering	p-type Si QD solar cell	525	33.7	78.5	13.4	[102]
VHF-PECVD	p-i-n device on quartz	518	0.34	0.58	—	[103]
Sputtering	(p) Si NC:SiC/(n) c-Si heterojunction solar cell	463	19	53	4.66	[104]
Sputtering	p-i-n device on quartz	373	—	—	—	[105]
PECVD	Si NC/SiC multilayer on membrane	180	0.1	28	5 × 10 ⁻³	[106]
	SiC monolayer on membrane	260	0.0025	59	2 × 10 ⁻⁴	
PECVD	Si QD tandem solar cell	978	0.2	—	—	[107]

Despite various fabrication strategies made to develop Si QDs in the Si-based dielectric matrix, the research outcome as described by different research groups are reported here for the implementation towards solar cell application. Significant growth parameters that affect the control of QD size and distribution density are thoroughly reviewed. For the realization of Si QD devices, selection of perfect Si-based matrix, the concentration of Si within the matrix, doping, control over precursor gases and finally annealing parameters play a crucial role. Control over these parameters gives an access to tune the crystallization process, phase separation, charge transport between the QDs and passivation of defect states to develop efficient solar cells.

In spite of continuous efforts made to control the growth of Si QDs, desired conversion efficiency for Si QD solar cell is infancy. Several reports confirmed a promising V_{oc} and fill factor which is still far behind that of a commercial solar cell. A maximum cell efficiency reported for Si QD solar cells is 13.4% with a V_{oc} of 525 mV [102]. This gap in the path of development may be fulfilled by a proper understanding of efficient synthesis method with a controllable growth of Si QDs within the dielectric matrix. Controllable growth may give an access to tune the bandgap and the conductivity of the solar cell absorber layer by controlling the size, interdot spacing and proper understanding of the role of doping in the QDs. Besides these, a proper realization of new device design with proper charge transport, QD superlattices, low defect states and interconnect is necessary. On the path to improve the V_{oc}, 'all-Si' tandem solar cell showed a promising result which opens the doorway for the practical realization of the new design for the Si QD solar cell. Though the result today is lower than as expected, but future studies on Si QD solar cell will definitely achieve a breakthrough to design a new promising Si QD solar cell.

Acknowledgement

This work is supported by the Korea Institute of Energy Technology Evaluation and Planning and the Ministry of Trade, Industry and Energy of the Republic of Korea (No. 20173010012940).

References

- Priolo, T. Gregorkiewicz, M. Galli, T.F. Krauss, Silicon nanostructures for photonics and photovoltaics, *Nat. Nanotechnol.* 9 (1) (2014) 19–32.
- W.A. Badawy, A review on solar cells from Si-single crystals to porous materials and quantum dots, *J. Adv. Res.* 6 (2) (2015) 123–132.
- M. Samadpour, Efficient CdS/CdSe/ZnS quantum dot sensitized solar cells prepared by ZnS treatment from methanol solvent, *Sol. Energy* 144 (2017) 63–70.
- Y. Xu, T. Gong, J.N. Munday, The generalized Shockley–Queisser limit for nanostructured solar cells, *Sci. Rep.* 5 (2015) 13536.
- N. Balaji, H.T. Nguyen, C. Park, M. Ju, J. Raja, S. Chatterjee, R. Jeyakumar, J. Yi, Electrical and optical characterization of SiO_xNy and SiO₂ dielectric layers and rear surface passivation by using SiO₂/SiO_xNy stack layers with screen printed local Al-BSF for c-Si solar cells, *Curr. Appl. Phys.* 18 (1) (2018) 107–113.
- M. Ju, N. Balaji, C. Park, H.T.T. Nguyen, J. Cui, D. Oh, M. Jeon, J. Kang, G. Shim, J. Yi, The effect of small pyramid texturing on the enhanced passivation and efficiency of single c-Si solar cells, *RSC Adv.* 6 (55) (2016) 49831–49838.
- P. Löper, M. Canino, D. Qazzazie, M. Schnabel, M. Allegrezza, C. Summonte, S.W. Glunz, S. Janz, M. Zacharias, Silicon nanocrystals embedded in silicon carbide: investigation of charge Carrier transport and recombination, *Appl. Phys. Lett.* 102 (3) (2013), 033507.
- L.T. Canham, Silicon quantum wire array fabrication by electrochemical and chemical dissolution of wafers, *Appl. Phys. Lett.* 57 (10) (1990) 1046–1048.
- L. Ding, T.P. Chen, Y. Liu, C.Y. Ng, Y.C. Liu, S. Fung, Thermal annealing effect on the band gap and dielectric functions of silicon nanocrystals embedded in SiO₂ matrix, *Appl. Phys. Lett.* 87 (12) (2005), 121903.
- M. Zacharias, J. Heitmann, R. Scholz, U. Kahler, M. Schmidt, J. Bläsing, Size-controlled highly luminescent silicon nanocrystals: a SiO/SiO₂ superlattice approach, *Appl. Phys. Lett.* 80 (4) (2002) 661–663.
- D. Di, H. Xu, I. Perez-Wurfl, M.A. Green, G. Conibeer, Improved nanocrystal formation, quantum confinement and Carrier transport properties of doped Si quantum dot superlattices for third generation photovoltaics, *Prog. Photovoltaics Res. Appl.* 21 (4) (2013) 569–577.
- Y.H. Cho, E.C. Cho, Y. Huang, C.W. Jiang, G. Conibeer, M.A. Green, Silicon quantum dots in SiN_x matrix for third generation photovoltaics, in: Proc 20th EU PVSEC, 2005, p. 47.
- I. Perez-Wurfl, L. Ma, D. Lin, X. Hao, M.A. Green, G. Conibeer, Silicon nanocrystals in an oxide matrix for thin film solar cells with 492mV open circuit voltage, *Sol. Energy Mater. Sol. Cells* 100 (2012) 65–68.
- C.W. Jiang, M.A. Green, Silicon quantum dot superlattices: modeling of energy bands, densities of states, and mobilities for silicon tandem solar cell applications, *J. Appl. Phys.* 99 (11) (2006), 114902.
- G. Conibeer, M. Green, R. Corkish, Y. Cho, E.C. Cho, C.W. Jiang, T. Fangsuwanarak, E. Pink, Y. Huang, T. Puzzer, T. Trupke, Silicon nanostructures for third generation photovoltaic solar cells, *Thin Solid Films* 511 (2006) 654–662.
- L.A. Nesbit, Annealing characteristics of Si-rich SiO₂ films, *Appl. Phys. Lett.* 46 (1) (1985) 38–40.
- A.K. Panchal, C.S. Solanki, Fabrication of silicon quantum dots in SiN_x multilayer using hot-wire CVD, *J. Cryst. Growth* 311 (9) (2009) 2659–2663.
- J. Zhu, W.T. Leach, S.K. Stanley, J.G. Ekerdt, X. Yan, Growth of high-density Si nanoparticles on Si₃N₄ and SiO₂ thin films by hot-wire chemical vapor deposition, *J. Appl. Phys.* 92 (8) (2002) 4695–4698.
- T.W. Kim, C.H. Cho, B.H. Kim, S.J. Park, Quantum confinement effect in crystalline silicon quantum dots in silicon nitride grown using SiH₄ and NH₃, *Appl. Phys. Lett.* 88 (12) (2006), 123102.
- H.L. Hao, L.K. Wu, W.Z. Shen, H.F.W. Dekkers, Origin of visible luminescence in hydrogenated amorphous silicon nitride, *Appl. Phys. Lett.* 91 (20) (2007), 201922.
- M. Molinari, H. Rinnert, M. Vergnat, Improvement of the photoluminescence properties in a-SiN_x films by introduction of hydrogen, *Appl. Phys. Lett.* 79 (14) (2001) 2172–2174.
- B. Abeles, T. Tiedje, Amorphous semiconductor superlattices, *Phys. Rev. Lett.* 51 (21) (1983), 2003.
- L. Brus, Zero-dimensional "excitons" in semiconductor clusters, *IEEE J. Quant. Electron.* 22 (9) (1986) 1909–1914.
- E.C. Cho, M.A. Green, G. Conibeer, D. Song, Y.H. Cho, G. Scardera, S. Huang, S. Park, X.J. Hao, Y. Huang, L. Van Dao, Silicon quantum dots in a dielectric matrix for all-silicon tandem solar cells, *Adv. Optoelectron.* 2007 (2007).
- L.X. Yi, J. Heitmann, R. Scholz, M. Zacharias, Phase separation of thin SiO layers in amorphous SiO/SiO₂ superlattices during annealing, *J. Phys. Condens. Matter* 15 (39) (2003) S2887.
- M. Molinari, H. Rinnert, M. Vergnat, P. Weisbecker, Evolution with annealing treatments of the size of silicon nanocrystallites embedded in a SiN_x matrix and correlation with optical properties, *Mater. Sci. Eng. B* 101 (1) (2003) 186–189.
- S. Ilday, G. Nogay, R. Turan, Spectroscopic ellipsometry study of Si nanocrystals embedded in a SiO_x matrix: modeling and optical characterization, *Appl. Surf. Sci.* 318 (2014) 256–261.
- J. Huang, Y. Zeng, W. Wang, Y. Yang, J. Huang, R. Tan, S. Dai, N. Dai, W. Song,

- Reduction of residual stress in SiO₂-matrix silicon nano-crystal thin films by a combination of rapid thermal annealing and tube-furnace annealing, *phys. status solidi A* 210 (3) (2013) 528–532.
- [29] X.J. Hao, A.P. Podhorodecki, Y.S. Shen, G. Zatryb, J. Misiewicz, M.A. Green, Effects of Si-rich oxide layer stoichiometry on the structural and optical properties of Si QD/SiO₂ multilayer films, *Nanotechnology* 20 (48) (2009), 485703.
- [30] P.D. Nguyen, D.M. Kepaptsoglou, Q.M. Ramasse, M.F. Sunding, L.O. Vestland, T.G. Finstad, A. Olsen, Impact of oxygen bonding on the atomic structure and photoluminescence properties of Si-rich silicon nitride thin films, *J. Appl. Phys.* 112 (7) (2012), 073514.
- [31] Y.H. So, S. Huang, G. Conibeer, M.A. Green, Formation and photoluminescence of Si nanocrystals in controlled multilayer structure comprising of Si-rich nitride and ultrathin silicon nitride barrier layers, *Thin Solid Films* 519 (16) (2011) 5408–5412.
- [32] Z. Wan, S. Huang, M.A. Green, G. Conibeer, Rapid thermal annealing and crystallization mechanisms study of silicon nanocrystal in silicon carbide matrix, *Nanoscale Res. Lett.* 6 (1) (2011) 129.
- [33] D. Song, E.C. Cho, G. Conibeer, Y. Huang, C. Flynn, M.A. Green, Structural characterization of annealed Si_{1-x}C_x/SiC multilayers targeting formation of Si nanocrystals in a SiC matrix, *J. Appl. Phys.* 103 (8) (2008), 083544.
- [34] X.J. Hao, E.C. Cho, G. Scardera, Y.S. Shen, E. Bellet-Amalric, D. Bellet, G. Conibeer, M.A. Green, Phosphorus-doped silicon quantum dots for all-silicon quantum dot tandem solar cells, *Sol. Energy Mater. Sol. Cells* 93 (9) (2009) 1524–1530.
- [35] Y. Kanazawa, M. Fujii, S. Hayashi, K. Yamamoto, Doping of B atoms into Si nanocrystals prepared by rf cosputtering, *Solid State Commun.* 100 (4) (1996) 227–230.
- [36] X. Jia, Z. Lin, T. Zhang, B. Puthen-Veettil, T. Yang, K. Nomoto, J. Ding, G. Conibeer, I. Perez-Wurfl, Accurate analysis of the size distribution and crystallinity of boron doped Si nanocrystals via Raman and PL spectra, *RSC Adv.* 7 (54) (2017) 34244–34250.
- [37] Y.H. So, S. Huang, G. Conibeer, M.A. Green, N-type conductivity of nanostructured thin film composed of antimony-doped Si nanocrystals in silicon nitride matrix, *Europhys. Lett.* 96 (1) (2011) 17011.
- [38] P.T. Huy, V.V. Thu, N.D. Chien, C.A.J. Ammerlaan, J. Weber, Structural and optical properties of Si-nanoclusters embedded in silicon dioxide, *Phys. B Condens. Matter* 376 (2006) 868–871.
- [39] V.V. Voitovych, R.M. Rudenko, A.G. Kolosiuk, M.M. Krasko, V.O. Juhimchuk, M.V. Voitovych, S.S. Ponomarov, A.M. Kraitchinskii, V.Y. Povarchuk, V.A. Makara, Effect of tin on the processes of silicon-nanocrystal formation in amorphous SiO_x thin-film matrices, *Semiconductors* 48 (1) (2014) 73–76.
- [40] D. Li, Y.B. Chen, M. Lu, An effect of laser pre-annealing on the enhancement of light emission of Si nanocrystal thin film, *Mater. Lett.* 89 (2012) 9–11.
- [41] K. Surana, H. Lepage, J.M. Lebrun, B. Doisneau, D. Bellet, L. Vandroux, G. Le Carval, M. Baudrit, P. Thony, P. Mur, Film-thickness-dependent conduction in ordered Si quantum dot arrays, *Nanotechnology* 23 (10) (2012), 105401.
- [42] Y. Li, B. Qian, Z. Sui, C. Jiang, Breakdown point of quantum confinement photoluminescence and space-separation dependent energy transfer from silicon nanocrystals, *Appl. Phys. Lett.* 103 (16) (2013), 161908.
- [43] X. Wang, X. Yu, W. Yu, H. Feng, J. Wang, C. Yin, W. Lu, G. Fu, Effects of annealing ambient on the photoluminescence properties of Si-rich oxide/SiO₂ multilayer films containing Si-nanocrystals, *J. Mater. Sci.* 49 (3) (2014) 1353–1358.
- [44] J. Barbe, K. Makasheva, S. Perraud, M. Carrada, B. Despax, Structural analysis of the interface of silicon nanocrystals embedded in a Si₃N₄ matrix, *J. Phys. D* 47 (25) (2014), 255302.
- [45] N.M. Park, C.J. Choi, T.Y. Seong, S.J. Park, Quantum confinement in amorphous silicon quantum dots embedded in silicon nitride, *Phys. Rev. Lett.* 86 (7) (2001) 1355.
- [46] D. Hiller, A. Zelenina, S. Gutsch, S.A. Dyakov, L. López-Conesa, J. López-Vidrier, S. Estradé, F. Peiró, B. Garrido, J. Valenta, M. Kořínek, Absence of quantum confinement effects in the photoluminescence of Si₃N₄-embedded Si nanocrystals, *J. Appl. Phys.* 115 (20) (2014), 204301.
- [47] G. Scardera, T. Puzzer, I. Perez-Wurfl, G. Conibeer, The effects of annealing temperature on the photoluminescence from silicon nitride multilayer structures, *J. Cryst. Growth* 310 (15) (2008) 3680–3684.
- [48] A.M. Hartel, M. Küngle, P. Löper, S. Janz, A.W. Bett, Amorphous Si x C 1 – x : H single layers before and after thermal annealing: correlating optical and structural properties, *Sol. Energy Mater. Sol. Cells* 94 (11) (2010) 1942–1946.
- [49] G. Wen, X. Zeng, W. Liao, C. Cao, Crystallization mechanism of silicon quantum dots upon thermal annealing of hydrogenated amorphous Si-rich silicon carbide films, *Thin Solid Films* 552 (2014) 18–23.
- [50] M. Küngle, S. Janz, K.G. Nickel, A. Heidt, M. Luysberg, O. Eibl, Annealing of nm-thin Si_{1-x}C_x/SiC multilayers, *Sol. Energy Mater. Sol. Cells* 115 (2013) 11–20.
- [51] D. Ma, J. Liu, W. Zhang, Investigation of silicon quantum dots embedded in boron-doped silicon oxide thin films prepared by PECVD applying Ar dilution, *Phys. Status Solidi* 215 (2) (2018), 1700682.
- [52] K. Nomoto, D. Hiller, S. Gutsch, A.V. Ceguerra, A. Breen, M. Zacharias, G. Conibeer, I. Perez-Wurfl, S.P. Ringer, Atom probe tomography of size-controlled phosphorus doped silicon nanocrystals, *Phys. Status Solidi Rapid Res. Lett.* 11 (1) (2017).
- [53] J. Ma, J. Ni, J. Zhang, Q. Liu, X. Chen, D. Zhang, X. Zhang, Y. Zhao, High open-circuit voltage (1.04 V) n-i-p type thin film silicon solar cell by two-phase silicon carbide intrinsic material, *Sol. Energy Mater. Sol. Cells* 130 (2014) 561–566.
- [54] N.R. Mavilla, C.S. Solanki, J. Vasi, Raman spectroscopy of silicon-nanocrystals fabricated by inductively coupled plasma chemical vapor deposition, *Physica E: Low Dimens. Syst. Nanostruct.* 52 (2013) 59–64.
- [55] Z.J. Horváth, P. Basa, P. Petrik, C. Dúcsó, T. Jászi, L. Dobos, L. Tóth, T. Lohner, B. Pécz, M. Fried, Si nanocrystals in sandwiched SiN_x structures, in: First Int. Workshop on Semiconductor Nanocrystals, SEMINANO2005, 2005, pp. 417–419.
- [56] K.M. Lee, T.H. Kim, J.D. Hwang, S. Jang, K. Jeong, M. Han, S. Won, J. Sok, K. Park, W.S. Hong, Size control of silicon nanocrystals in silicon nitride film deposited by catalytic chemical vapor deposition at a low temperature (< 200° C), *Scr. Mater.* 60 (8) (2009) 703–705.
- [57] Z.H. Lu, D.J. Lockwood, J.M. Baribeau, Quantum confinement and light emission in SiO₂/Si superlattices, *Nature* 378 (6554) (1995) 258–260.
- [58] W.M. Chen, I.A. Buyanova, W.X. Ni, G.V. Hansson, B. Momemar, Identification of grown-in efficient nonradiative recombination centers in molecular beam epitaxial silicon, *Phys. Rev. Lett.* 77 (20) (1996) 4214.
- [59] L.N. Dinh, L.L. Chase, M. Balooch, L.J. Terminello, F. Wooten, Photoluminescence of oxidized silicon nanoclusters deposited on the basal plane of graphite, *Appl. Phys. Lett.* 65 (24) (1994) 3111–3113.
- [60] J. Gan, Q. Li, Z. Hu, W. Yu, K. Gao, J. Sun, N. Xu, J. Wu, Study on phase separation in a-SiO_x for Si nanocrystal formation through the correlation of photoluminescence with structural and optical properties, *Appl. Surf. Sci.* 257 (14) (2011) 6145–6151.
- [61] R. Karmouch, G. Savard, D. Barba, D. Koshele, F. Martin, G.G. Ross, Investigation of electrical and optical measurements of silicon nanocrystals embedded in SiO₂ matrix, *J. Mater. Sci. Mater. Electron.* 24 (6) (2013) 1837–1841.
- [62] L. Yi, R. Scholz, M. Zacharias, Size and density control of Si-nanocrystals realized by SiO_x/SiO₂ superlattice, *J. Lumin.* 122 (2007) 750–752.
- [63] T. Baron, F. Martin, P. Mur, C. Wyon, M. Dupuy, C. Busseret, A. Souifi, G. Guillot, Low pressure chemical vapor deposition growth of silicon quantum dots on insulator for nanoelectronics devices, *Appl. Surf. Sci.* 164 (1) (2000) 29–34.
- [64] K. Chen, M. Wang, W. Shi, L. Jiang, W. Li, J. Xu, X. Huang, Visible electroluminescence from crystallized a-Si:H/a-SiN_x: H multiquantum well structures, *J. Non-Cryst. Solids* 198 (1996) 833–836.
- [65] L. Zhang, K. Chen, L. Wang, W. Li, J. Xu, X. Huang, K. Chen, The dependence of the interface and shape on the constrained growth of nc-Si in a-SiN_x/a-Si: H/a-SiN_x structures, *J. Phys. Condens. Matter* 14 (43) (2002) 10083.
- [66] M. Küngle, A. Hartel, S. Janz, Preparation of si-quantumdots in sic: single layer vs multi layer approach, in: Proc. 23rd European Photovoltaic Solar Energy Conference and Exhibition, 2008, pp. 421–425.
- [67] A.M. Hartel, D. Hiller, S. Gutsch, P. Löper, S. Estradé, F. Peiró, B. Garrido, M. Zacharias, Formation of size-controlled silicon nanocrystals in plasma enhanced chemical vapor deposition grown SiO_x Ny/SiO₂ superlattices, *Thin Solid Films* 520 (1) (2011) 121–125.
- [68] U. Kahler, H. Hofmeister, Visible light emission from Si nanocrystalline composites via reactive evaporation of SiO, *Opt. Mater.* 17 (1) (2001) 83–86.
- [69] J. Huang, C. Gui, M. Ding, H. Wang, W. Xu, J. Li, M. Gao, H. Guan, Effects of chemical stoichiometry on the structural properties of Si-rich oxide thin films, *Thin Solid Films* 595 (2015) 79–83.
- [70] B. Rezgui, A. Sibai, T. Nychiporuk, M. Lemiti, G. Brémond, Photoluminescence and optical absorption properties of silicon quantum dots embedded in Si-rich silicon nitride matrices, *J. Lumin.* 129 (12) (2009) 1744–1746.
- [71] A.K. Panchal, D.K. Rai, M. Mathew, C.S. Solanki, Photovoltaic devices with silicon quantum wells and dots structures in silicon nitride dielectric, in: Proc. 26th EU PVSEC, 2011, pp. 41–43.
- [72] D. Song, E.C. Cho, G. Conibeer, Y.H. Cho, Y. Huang, S. Huang, C. Flynn, M.A. Green, Fabrication and characterization of Si nanocrystals in SiC matrix produced by magnetron co-sputtering, *J. Vac. Sci. Technol. B: Microelectron. Nanometer. Struct. Process. Meas. Phenom.* 25 (4) (2007) 1327–1335.
- [73] Y.H. Cho, D. Song, E.C. Cho, G. Scardera, Y. Huang, S. Park, S. Lee, E. Lee, S. Huang, G. Conibeer, M.A. Green, Silicon quantum dot superlattices in SiC matrix for all silicon tandem cells, in: Proc. 17th PVSEC, 2007.
- [74] B.J. Hinds, F. Wang, D.M. Wolfe, C.L. Hinkle, G. Lucovsky, Investigation of post oxidation thermal treatments of Si/SiO₂ interface in relationship to the kinetics of amorphous Si suboxide decomposition, *J. Vac. Sci. Technol. B: Microelectron. Nanometer. Struct. Process. Meas. Phenom.* 16 (4) (1998) 2171–2176.
- [75] J. Laube, S. Gutsch, D. Hiller, M. Bruns, C. Kübel, C. Weiss, M. Zacharias, Formation of size controlled silicon nanocrystals in nitrogen free silicon dioxide matrix prepared by plasma enhanced chemical vapor deposition, *J. Appl. Phys.* 116 (22) (2014), 223501.
- [76] E.G. Barbagiovanni, D.J. Lockwood, P.J. Simpson, L.V. Goncharova, Quantum confinement in Si and Ge nanostructures: theory and experiment, *Appl. Phys. Rev.* 1 (1) (2014), 011302.
- [77] C. Summonte, M. Canino, M. Allegrezza, M. Bellettato, A. Desalvo, S. Mirabella, A. Terrasi, Systematic characterization of Silicon nanodot absorption for third-generation photovoltaics, in: Proc. 26th EU PVSEC, 2011, p. 361.
- [78] Y. Kurokawa, S. Miyajima, A. Yamada, M. Konagai, Preparation of nanocrystalline silicon in amorphous silicon carbide matrix, *Jpn. J. Appl. Phys.* 45 (10L) (2006) L1064.
- [79] D.J. Norris, N. Yao, F.T. Charnock, T.A. Kennedy, High-quality manganese-doped ZnSe nanocrystals, *Nano Lett.* 1 (1) (2001) 3–7.

- [80] G.M. Dalpian, J.R. Chelikowsky, Self-purification in semiconductor nanocrystals, *Phys. Rev. Lett.* 96 (22) (2006), 226802.
- [81] S.C. Erwin, L. Zui, M.I. HafTEL, A.L. Efros, T.A. Kennedy, D.J. Norris, Doping semiconductor nanocrystals, *Nature* 436 (7047) (2005) 91–94.
- [82] M. Xie, D. Li, L. Chen, F. Wang, X. Zhu, D. Yang, The location and doping effect of boron in Si nanocrystals embedded silicon oxide film, *Appl. Phys. Lett.* 102 (12) (2013), 123108.
- [83] J. Ma, J. Ni, J. Zhang, Z. Huang, G. Hou, X. Chen, X. Zhang, X. Geng, Y. Zhao, Improvement of solar cells performance by boron doped amorphous silicon carbide/nanocrystalline silicon hybrid window layers, *Sol. Energy Mater. Sol. Cells* 114 (2013) 9–14.
- [84] M. Fujii, S. Hayashi, K. Yamamoto, Photoluminescence from B-doped Si nanocrystals, *J. Appl. Phys.* 83 (12) (1998) 7953–7957.
- [85] Y. Zeng, N. Dai, Q. Cheng, J. Huang, X. Liang, W. Song, Preparation and characterization of phosphorus-doped silicon nanocrystals in SiC x films, *Mater. Sci. Semicond. Process.* 16 (3) (2013) 598–604.
- [86] P.J. Wu, Y.C. Wang, I.C. Chen, Fabrication of Si heterojunction solar cells using P-doped Si nanocrystals embedded in SiN x films as emitters, *Nanoscale Res. Lett.* 8 (1) (2013) 457.
- [87] A. Mimura, M. Fujii, S. Hayashi, D. Kovalev, F. Koch, Photoluminescence and free-electron absorption in heavily phosphorus-doped Si nanocrystals, *Phys. Rev. B* 62 (19) (2000) 12625.
- [88] M. Fujii, A. Mimura, S. Hayashi, K. Yamamoto, Photoluminescence from Si nanocrystals dispersed in phosphosilicate glass thin films: improvement of photoluminescence efficiency, *Appl. Phys. Lett.* 75 (2) (1999) 184–186.
- [89] K. Nomoto, H. Sugimoto, A. Breen, A.V. Ceguerra, T. Kanno, S.P. Ringer, I.P. Wurfl, G. Conibeer, M. Fujii, Atom probe tomography analysis of boron and/or phosphorus distribution in doped silicon nanocrystals, *J. Phys. Chem. C* 120 (31) (2016) 17845–17852.
- [90] X.J. Hao, E.C. Cho, C. Flynn, Y.S. Shen, G. Conibeer, M.A. Green, Effects of boron doping on the structural and optical properties of silicon nanocrystals in a silicon dioxide matrix, *Nanotechnology* 19 (42) (2008) 424019.
- [91] T. Zhang, B. Simonds, K. Nomoto, B. Puthen Veettil, Z. Lin, I. Perez Wurfl, G. Conibeer, Pulsed KrF excimer laser dopant activation in nanocrystal silicon in a silicon dioxide matrix, *Appl. Phys. Lett.* 108 (8) (2016) 083103.
- [92] J.H. Yoon, Enhanced formation of Si nanocrystals in silicon-rich oxide implanted with Ni, *Mater. Lett.* 136 (2014) 237–240.
- [93] P.D. Persans, A. Ruppert, B. Abeles, Crystallization kinetics of amorphous Si/SiO₂ superlattice structures, *J. Non-Cryst. Solids* 102 (1–3) (1988) 130–135.
- [94] M. Zacharias, P. Streitenberger, Crystallization of amorphous superlattices in the limit of ultrathin films with oxide interfaces, *Phys. Rev. B* 62 (12) (2000) 8391.
- [95] S. Miyazaki, Y. Ihara, M. Hirose, Structural stability of amorphous semiconductor superlattices, *J. Non-Cryst. Solids* 97 (1987) 887–890.
- [96] A.R. Wilkinson, R.G. Elliman, The effect of annealing environment on the luminescence of silicon nanocrystals in silica, *J. Appl. Phys.* 96 (2004) 4018.
- [97] M. Bolduc, G. Genard, M. Yedji, D. Barba, F. Martin, G. Tervagne, G.G. Ross, Influence of nitrogen on the growth and luminescence of silicon nanocrystals embedded in silica, *J. Appl. Phys.* 105 (1) (2009) 013108.
- [98] D. Hiller, S. Goetze, M. Zacharias, Rapid thermal annealing of size-controlled Si nanocrystals: dependence of interface defect density on thermal budget, *J. Appl. Phys.* 109 (5) (2011) 054308.
- [99] M.A. Green, *Third Generation Photovoltaics*, Springer, New York, 2006.
- [100] G. Conibeer, *Third-generation photovoltaics*, *Mater. Today* 10 (11) (2007) 42–50.
- [101] E.C. Cho, S. Park, X. Hao, D. Song, G. Conibeer, S.C. Park, M.A. Green, Silicon quantum dot/crystalline silicon solar cells, *Nanotechnology* 19 (24) (2008) 245201.
- [102] S.H. Hong, Y.S. Kim, W. Lee, Y.H. Kim, J.Y. Song, J.S. Jang, J.H. Park, S.H. Choi, K.J. Kim, Active doping of B in silicon nanostructures and development of a Si quantum dot solar cell, *Nanotechnology* 22 (42) (2011) 425203.
- [103] S. Yamada, Y. Kurokawa, S. Miyajima, M. Konagai, Silicon quantum dot superlattice solar cell structure including silicon nanocrystals in a photo-generation layer, *Nanoscale Res. Lett.* 9 (1) (2014) 246.
- [104] D. Song, E.C. Cho, G. Conibeer, C. Flynn, Y. Huang, M.A. Green, Structural, electrical and photovoltaic characterization of Si nanocrystals embedded SiC matrix and Si nanocrystals/c-Si heterojunction devices, *Sol. Energy Mater. Sol. Cells* 92 (4) (2008) 474–481.
- [105] I. Perez-Wurfl, X. Hao, A. Gentle, D.H. Kim, G. Conibeer, M.A. Green, Si nanocrystal p-i-n diodes fabricated on quartz substrates for third generation solar cell applications, *Appl. Phys. Lett.* 95 (15) (2009) 153506.
- [106] J. López-Vidrier, P. López, M. Schnabel, S. Hernández, M. Canino, C. Summonte, S. Janz, B. Garrido, Silicon nanocrystals embedded in silicon carbide as a wide-band gap photovoltaic material, *Sol. Energy Mater. Sol. Cells* 144 (2016) 551–558.
- [107] S. Janz, M. Schnabel, P. López, C. Summonte, M. Canino, J. López-Vidrier, S. Hernández, B. Garrido, S.W. Glunz, Processing and characterisation of tandem solar cells from crystalline silicon materials, in: 28th EU PVSEC, 2013, pp. 142–146.
- [108] G. Conibeer, S. Shrestha, S. Huang, R. Patterson, H. Xia, Y. Feng, P. Zhang, N. Gupta, M. Tayebjee, S. Smyth, Y. Liao, Hot Carrier solar cell absorber prerequisites and candidate material systems, *Sol. Energy Mater. Sol. Cells* 135 (2015) 124–129.